Exact Error-Rate Analysis of Diversity 16-QAM With Channel Estimation Error

Lingzhi Cao, *Member, IEEE,* and Norman C. Beaulieu, *Fellow, IEEE*

***Abstract*—The bit-error rate (BER) performance of multilevel quadrature amplitude modulation with pilot-symbol-assisted modulation channel estimation in static and Rayleigh fading channels is derived, both for single branch reception and maximal ratio combining diversity receiver systems. The effects of noise and estimator decorrelation on the received BER are examined. The high sensitivity of diversity systems to channel estimation error is investigated and quantified. The influence of the pilot-symbol interpolation filter windowing is also considered.**

***Index Terms*—Diversity, estimation error, fading channels, maximal ratio combining (MRC), pilot-symbol-assisted modulation (PSAM), quadrature amplitude modulation (QAM).**

I. Introduction

THE performances of multilevel quadrature amplitude modulation (M-QAM) in different wireless environments have been studied by several authors. [1] gives the bit-error rate (BER) of 16-QAM and 64-QAM over both the additive white Gaussian noise (AWGN) channel and the Rayleigh fading channel without diversity. A recursive algorithm for computing the BER of M-QAM constellations over an AWGN channel was given in [2]. Much work has focused on the derivation of the symbol-error rate (SER) when diversity techniques are used to compensate for the fading caused by the multipath propagation. [3] presented the SER of M-QAM with maximal ratio combining (MRC) diversity and selection combining (SC) diversity in Rayleigh fading channels. In [4], precise analytical expressions for the SER of MRC and equal gain combining (EGC) in Nakagami fading channels were derived. [5] gave a thorough study of the performances of two-dimensional signaling schemes. The SER of 16-QAM on Rayleigh, Ricean, and Nakagami fading channels with MRC, EGC, and SC was derived. The SER for M-QAM with MRC reception was given in terms of alternate forms of the Q-functions, widely used in communication theory in [6].

References [1]–[6] assume that perfect channel state information (CSI) is available to the receivers. Meanwhile, the performances of coherent demodulation and coherent combining can be severely degraded if good fading CSI is not available, as shown in [7]. Study of a variable-rate, variable-power M-QAM in [8] also showed the sensitivity of the error rate of M-QAM to estimation error.

Pilot-symbol-assisted modulation (PSAM) has proved to be an effective method for channel estimation [9], [10]. Some previous work has considered the performance of M-QAM when using PSAM for channel estimation. [11] gives simple upper bounds for the SER of M-QAM over a Rayleigh fading channel in the presence of channel estimation error, and the approximate BER of M-QAM with imperfect channel estimation has been derived in [12]. None of [7], [8], [11], or [12] considered diversity QAM. In this paper, we derive the BER of 16-QAM using PSAM to provide estimates of the channel amplitude and phase in the receiver demodulation process for AWGN and Rayleigh fading channels, and for MRC diversity systems, in which case, the PSAM is used to provide CSI for both the demodulation process and the diversity combining. Though we consider specifically 16-QAM, the analysis is general and can be applied to general M-QAM with minor modifications, but more cumbersome definitions, notations, and development.

This paper is organized as follows. In Section II, the system model as well as the 16-QAM modulation are described, and some parameters used in the later sections are derived. The BER performance of 16-QAM in AWGN and in fading is derived in Section III and the limitations of previous work are clarified. In Section IV, the BER of 16-QAM with MRC diversity is derived. Some examples calculated using our theoretical results are presented and discussed in Section V. Simulation results are also presented for verification. Section VI concludes the paper.

II. System and Channel Models

A. PSAM

The PSAM system structure considered here is identical to that considered in [12], and the reader is referred to [12, Figs. 1, 3, and 7]. A block diagram of the PSAM system structure considered here is shown in [12, Fig. 1]. The transmitter periodically inserts the known pilot symbols into the data sequence via a multiplexer. Let s_k^l denote the lth symbol transmitted in the kth data frame. The symbols are formatted into frames of L symbols, with the first pilot symbol ($l = 0$) followed by $(L-1)$ data symbols ($1 \leq l \leq L-1$), as depicted in [12, Fig. 7]. At the receiver side, the pilot symbols are extracted and input to an estimation/interpolator filter. Thus, knowledge of the channel amplitude and phase at the times of the pilot symbols is used to estimate the channel amplitude and phase at the times of other symbols.

Paper approved by P. Y. Kam, the Editor for Modulation and Detection for Wireless Systems of the IEEE Communications Society. Manuscript received March 12, 2003; revised October 2, 2003 and December 12, 2003.

The authors are with the Department of Electrical and Computer Engineering, University of Alberta, Edmonton, AB T6G 2V4, Canada (e-mail: lingzhi@ee.ualberta.ca; beaulieu@ee.ualberta.ca)

Digital Object Identifier 10.1109/TCOMM.2004.829516

0090-6778/04$20.00 © 2004 IEEE

Denote the symbol interval as T and assume perfect symbol timing recovery. The received signal sample at the lth symbol in the kth frame, r_k^l, is given by

$$r_k^l = g_k^l s_k^l + n_k^l \tag{1}$$

where $g_k^l = \alpha_k^l e^{j\theta_k^l}$ is the complex channel gain sample with Rayleigh-distributed amplitude sample, α_k^l, and phase sample θ_k^l uniformly distributed on $[0, 2\pi)$; s_k^l is the transmitted 16-QAM signal sample, and n_k^l is the AWGN sample with variance σ_n in both the real and imaginary parts. The channel estimate for the kth pilot symbol, $\hat{p}_k$, is given by

$$\hat{p}_k = p_k + \frac{n_k^0}{s_p} \tag{2}$$

where p_k is the complex channel gain corresponding to the pilot symbol in the kth frame, and s_p is the known pilot symbol in the kth frame. The fading at the lth symbol in the kth frame is estimated from K adjacent pilot symbols with k_1 pilot symbols from previous frames, one from the current frame, and k_2 pilot symbols from subsequent frames, where $k_1 + k_2 + 1 = K$. The estimate is given by

$$\hat{g}_k^l = \hat{\alpha}_k^l e^{j\hat{\theta}_k^l} = \sum_{m=-k_1+k}^{k_2+k} h_m^l \hat{p}_m \tag{3}$$

where $h_m^l, l = 0, 1, \ldots, L-1, m = -k_1+k, \ldots, 0, \ldots, k_2+k$ are the interpolation coefficients of the estimation filter [10].

Since the channel fading and the noise are independent complex Gaussian random variables, the channel estimate $\hat{g}_k^l$, which is a weighted sum of zero-mean complex jointly Gaussian random variables, is also a zero-mean complex Gaussian random variable [13, Ch. 8], [14, Ch. 6]. Since g_k^l and $\hat{g}_k^l$ are correlated complex Gaussian random variables, the joint probability density function (jpdf) of their amplitudes, α_k^l and $\hat{\alpha}_k^l$, and their phase difference, φ_k^l, can be derived following the discussion given in [13, Ch. 8]. The subscripts for the complex channel gain and its estimate have been omitted in the following discussion when ambiguity can not arise, for notational simplicity. Similarly, the dependence on τ, the time difference between two samples, has also been suppressed for notational brevity. The jpdf, $p(\alpha, \hat{\alpha}, \varphi)$, given in [13, eq. (8–102)], is with the notation used here

$$p(\alpha, \hat{\alpha}, \varphi) = \frac{\alpha\hat{\alpha}}{2\pi|\wedge|^{1/2}} \exp\left\{-\frac{[\sigma_{\hat{x}}^2\alpha^2 + \sigma_x^2\hat{\alpha}^2 - 2R_c\alpha\hat{\alpha}\cos\varphi - 2R_{cs}\alpha\hat{\alpha}\sin\varphi]}{2|\wedge|^{1/2}}\right\} \tag{4a}$$

where

$$\sigma_x^2 = E[g_I^2] = E[g_Q^2] \tag{4b}$$

$$\sigma_{\hat{x}}^2 = E[\hat{g}_I^2] = E[\hat{g}_Q^2] \tag{4c}$$

$$R_c = E[g_I\hat{g}_I] = E[g_Q\hat{g}_Q] \tag{4d}$$

$$R_{cs} = E[g_I\hat{g}_Q] = -E[g_Q\hat{g}_I] \tag{4e}$$

$$|\wedge| = [\sigma_x^2\sigma_{\hat{x}}^2 - R_c^2 - R_{cs}^2]^2. \tag{4f}$$

The second-order joint central moments, R_c and R_{cs}, are derived in Section II-B, and $\sigma_{\hat{x}}^2$ is derived in Section II-C.

B. Derivation of the Covariance Between g and $\hat{g}$

The complex fading gain can be expressed in terms of quadrature components as

$$g(t) = g_I(t) + jg_Q(t). \tag{5}$$

In an omnidirectional scattering Rayleigh fading channel, the autocorrelation and cross-correlation are given by [15]

$$R(\tau) = R_{g_I}(\tau) = R_{g_Q}(\tau) = \sigma_x^2 J_0(2\pi f_D\tau) \tag{6}$$

and

$$R_{IQ}(\tau) = E[g_I(t)g_Q(t+\tau)] = 0 \tag{7}$$

respectively, where $J_0(\cdot)$ is the zeroth-order Bessel function of the first kind [16] and f_D is the maximum Doppler frequency.

Using (2), (3), (6), and (7) in (4d) and (4e), the covariances, R_c and R_{cs}, are determined as

$$R_c = E[g_I\hat{g}_I] = \sum_{k=-k_1}^{k_2} h_k^l E\left[g_I\left(p_{Ik} + \mathrm{Re}\left\{\frac{n_k^0}{s_p}\right\}\right)\right] = \sum_{k=-k_1}^{k_2} \sigma_x^2 h_k^l J_0(2\pi f_D|kL - l|T_s) \tag{8a}$$

$$R_{cs} = E[g_I\hat{g}_Q] = \sum_{k=-k_1}^{k_2} h_k^l E\left[g_I\left(p_{Qk} + \mathrm{Im}\left\{\frac{n_k^0}{s_p}\right\}\right)\right] = 0. \tag{8b}$$

C. Derivation of $\sigma_{\hat{x}}^2$

The variance of each component of the complex Gaussian fading estimate is obtained by using the definition (4c) with (2) and (3). It is given by

$$\sigma_{\hat{x}}^2 = E[\hat{g}_I^2] = E[\hat{g}_Q^2] = \sum_k \sum_m h_k^l h_m^l \mathrm{cov}(p_{Ik}p_{Im}) + \sum_k (h_k^l)^2 \frac{\sigma_n^2}{|s_p|^2}. \tag{9}$$

From (6)

$$\mathrm{cov}(p_{Ik}p_{Im}) = R(|k-m|LT_s) = \sigma_x^2 J_0(2\pi f_D|k-m|LT_s) \tag{10}$$

and assuming that the pilot-symbol energy E_p is equal to the average data symbol energy E_s, one can rewrite (9) as

$$\sigma_{\hat{x}}^2 = \sum_k \sum_m h_k^l h_m^l R(|k-m|LT_s) + \sum_k (h_k^l)^2 \frac{\sigma_n^2}{E_s} = H_l R H_l' + |H_l|^2 \frac{\sigma_n^2}{E_s}. \tag{11}$$

The results of (8a), (8b), and (11) are used in the jpdf (4a) of the amplitudes and phase difference of the channel fading and its estimate.

D. Modulation and Demodulation of Square QAM

[1] describes the modulation and demodulation of square M-QAM. The signaling constellation and the Gray code mapping of the transmitted bits is shown in [12, Fig. 3]. The transmitted bits are first split into in-phase (I) and quadrature (Q) bit streams to modulate the I and Q carriers. The demodulation of the received signal is implemented by extracting the I and Q components separately, and deciding the transmitted

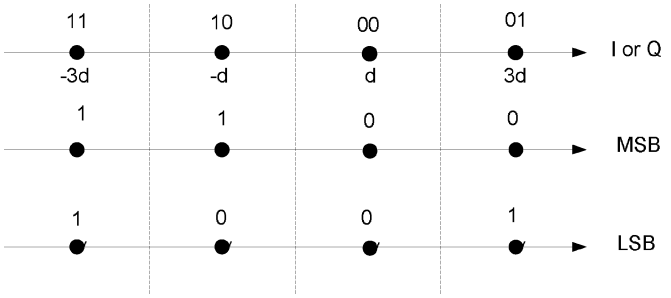

Fig. 1. 16-QAM I and Q bit demappings (after [12, Fig. 5]).

bits according to the decision boundaries. In the 16-QAM constellation, every symbol is represented by four bits in the sequence of i_1, q_1, i_2, q_2, where i_1 and i_2 are the in-phase bits and q_1 and q_2 are the quadrature bits. The I and Q bit streams are Gray encoded by assigning the bits 01, 00, 10, 11 to the levels $3d$, d, $-d$, and $-3d$, respectively, where d is the decision distance, shown in Fig. 1. Due to the symmetry of the constellation, the demodulation scheme is same for the I and Q components. Each symbol has two most significant bits (MSBs) i_1 and q_1, and two least significant bits (LSBs) i_2 and q_2. Following the analysis in [1], we calculate the MSB BER P_M, and the LSB BER P_L, separately. Then, the BER P_e of 16-QAM is the average of P_M and P_L. That is

$$P_e = \frac{1}{2}\left(P_M + P_L\right). \tag{12}$$

The BER with channel estimation error is derived in the next section.

III. BER Performance Analysis

The BER of 16-QAM with channel estimation error is determined by averaging the conditional error rate, conditioned on the channel amplitude, channel amplitude estimate, and channel phase estimate error, across the channel amplitude, channel amplitude estimate, and channel phase estimate error. The information symbols are assumed to be transmitted with the same probability. By symmetry, the BERs for the I and Q bit streams are the same. We consider estimation that is both corrupted by AWGN and by decorrelations between an information symbol and the pilot symbols caused by the time-varying fading. We also account for the cross-quadrature-carrier intersymbol interference (ISI) that occurs because of the phase error.

In the case of perfect channel estimation, the receiver can construct the decision boundaries perfectly. However, in the case of imperfect channel estimation, the decision boundaries are set with the imperfect channel estimate. The situation is shown in Fig. 2, where it is illustrated that the phase error causes rotation of the decision boundaries. Further clarification is provided in Fig. 3; the true phase is θ and the estimated phase is $\hat{\theta}$; so, there is a phase error φ. The phase error causes a signal amplitude degradation, replacing, for example, $3\alpha d$ by $3\alpha d\cos\varphi$. The phase error also causes cross-quadrature ISI with values $\pm 3d\alpha\sin\varphi$ or $\pm d\alpha\sin\varphi$. Note further that due to the symmetries and sign changes of $(+3d\alpha\sin\varphi, -3d\alpha\sin\varphi)$ and $(+d\alpha\sin\varphi, -d\alpha\sin\varphi)$, it suffices to include only the values $(3d\alpha\sin\varphi, d\alpha\sin\varphi)$ in the BER averaging.

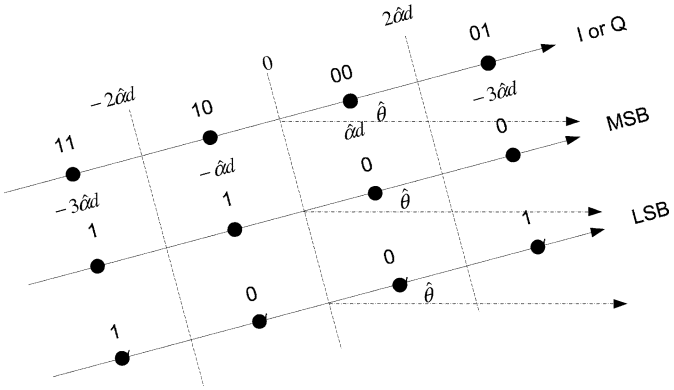

Fig. 2. New decision boundaries set by the imperfect estimate. The coordinates are those relative to the rotated signal constellation.

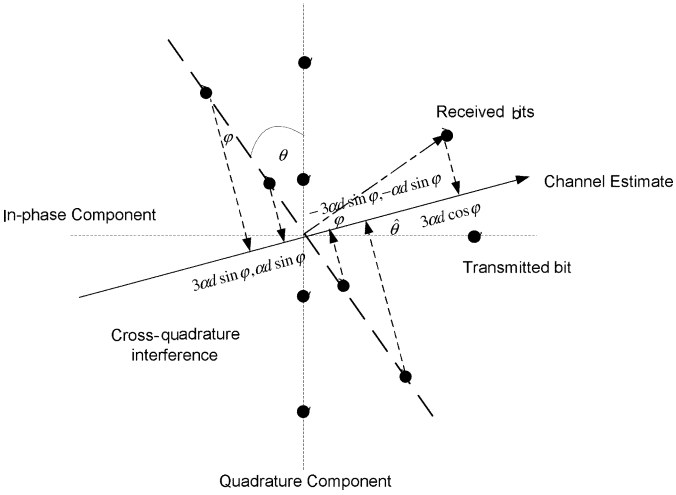

Fig. 3. Cross-quadrature interferences due to imperfect estimation.

It is informative to compare these with the decision boundaries shown in Fig. 1 for the case of perfect channel estimation. As seen in Fig. 1, the decision boundary for the MSB bits is zero with perfect estimation. This decision boundary is the same with imperfect estimation, as the fading amplitude does not affect the decision boundary in the MSB case, as also seen in Fig. 2. The BER of the MSB conditioned on α, $\hat{\alpha}$, and φ, and accounting for the ISI from the cross-quadrature components, is

$$\begin{aligned} P_M(e|\alpha,\hat{\alpha},\varphi) &= \frac{1}{4}\left\{ Q\left[\frac{d}{\sigma_n}(3\alpha\cos\varphi + 3\alpha\sin\varphi)\right] \right. \\ &\quad + Q\left[\frac{d}{\sigma_n}(3\alpha\cos\varphi + \alpha\sin\varphi)\right] \\ &\quad + Q\left[\frac{d}{\sigma_n}(\alpha\cos\varphi + 3\alpha\sin\varphi)\right] \\ &\quad \left. + Q\left[\frac{d}{\sigma_n}(\alpha\cos\varphi + \alpha\sin\varphi)\right]\right\} \end{aligned} \tag{13}$$

where $Q(x), x \geq 0$ is the complementary error function [17], [18]; when $x < 0$, $Q(x) = 1 - Q(|x|)$. As seen in Fig. 1, the decision boundaries for the LSBs are located at $\pm 2\alpha d$ under the assumption that the channel information is perfectly known. In

the presence of channel estimation error, the decision boundaries are located at $\pm 2\hat{\alpha}d$, as shown in Fig. 2. If a demodulated quadrature sample amplitude is greater than $|2\hat{\alpha}d|$, it is mapped to "1"; if it is greater than $-2\hat{\alpha}d$ and less than $+2\hat{\alpha}d$, it is mapped to "0". Thus, when a logical "1" is transmitted, the conditional BER can be expressed as $Q[(3\alpha d\cos\varphi - 2\hat{\alpha}d)/\sigma_n] - Q[(3\alpha d\cos\varphi + 2\hat{\alpha}d)/\sigma_n]$; when a logical "0" is transmitted, the conditional BER is given by $Q[(2\hat{\alpha}d - \alpha d\cos\varphi)/\sigma_n] + Q[(2\hat{\alpha}d + \alpha d\cos\varphi)/\sigma_n]$. The BER of the LSB conditioned on α, $\hat{\alpha}$, and φ and accounting for the cross-quadrature interference, is then

$$\begin{aligned} P_L(e|\alpha,\hat{\alpha},\varphi) = \frac{1}{4}\Bigg\{ & Q\left[\frac{d}{\sigma_n}(3\alpha\cos\varphi + 3\alpha\sin\varphi - 2\hat{\alpha})\right] \\ & - Q\left[\frac{d}{\sigma_n}(3\alpha\cos\varphi + 3\alpha\sin\varphi + 2\hat{\alpha})\right] \\ & + Q\left[\frac{d}{\sigma_n}(3\alpha\cos\varphi + \alpha\sin\varphi - 2\hat{\alpha})\right] \\ & - Q\left[\frac{d}{\sigma_n}(3\alpha\cos\varphi + \alpha\sin\varphi + 2\hat{\alpha})\right] \\ & + Q\left[\frac{d}{\sigma_n}(-\alpha\cos\varphi + 3\alpha\sin\varphi + 2\hat{\alpha})\right] \\ & + Q\left[\frac{d}{\sigma_n}(\alpha\cos\varphi + 3\alpha\sin\varphi + 2\hat{\alpha})\right] \\ & + Q\left[\frac{d}{\sigma_n}(-\alpha\cos\varphi + \alpha\sin\varphi + 2\hat{\alpha})\right] \\ & + Q\left[\frac{d}{\sigma_n}(\alpha\cos\varphi + \alpha\sin\varphi + 2\hat{\alpha})\right]\Bigg\} \end{aligned} \tag{14a}$$

$$10d^2 = E_s \tag{14b}$$

$$E_s = 4E_b \tag{14c}$$

$$\bar{\gamma}_b = \frac{2\sigma_x^2 E_b}{2\sigma_n^2} \tag{14d}$$

$$\left(\frac{d}{\sigma_n}\right)^2 = \sqrt{\frac{\frac{E_s}{10}}{\sigma_n^2}} = \frac{2\bar{\gamma}_b}{5\sigma_x^2} \tag{14e}$$

where E_b is the energy per bit and $\bar{\gamma}_b$ is the average signal-to-noise ratio (SNR) per bit.

Define the integral (15) as shown at the bottom of the page. Then, (15) combined with (12), (13), and (14) gives

$$P_e = \frac{1}{8}\sum_{i=1}^{12} w_i I(x_i, y_i, z_i, \bar{\gamma}_b, r, R_c) \tag{16}$$

TABLE I
COEFFICIENTS IN BER EXPRESSION (16) AND (37) FOR 16-QAM

i	w_i	x_i	y_i	z_i	i	w_i	x_i	y_i	z_i
1	1	3	3	0	7	-1	3	3	2
2	1	3	1	0	8	-1	3	1	2
3	1	1	3	0	9	1	-1	3	2
4	1	1	1	0	10	1	-1	1	2
5	1	3	3	-2	11	1	1	3	2
6	1	3	1	-2	12	1	1	1	2

where the coefficients w_i, x_i, y_i, z_i are listed in Table I. Define the integral $W1(x_i, y_i) = I(x_i, y_i, 0)$. $W1(x_i, y_i)$ can be simplified into a single integration by integrating over α and $\hat{\alpha}$, as shown in (17a) at the bottom of the page, where

$$\mu_1 = \frac{\sigma_{\hat{x}}^2}{2|\wedge|^{1/2}} \tag{17b}$$

$$\mu_2 = \frac{\sigma_x^2}{2|\wedge|^{1/2}} \tag{17c}$$

$$\nu = \frac{R_c}{|\wedge|^{1/2}} \tag{17d}$$

$$a = \sqrt{\frac{\gamma_b}{5\sigma_x^2}}(x_i\cos\varphi + y_i\sin\varphi) \tag{17e}$$

$$b^2 = \mu_1 - \frac{(\nu\cos\varphi)^2}{4\mu_2}. \tag{17f}$$

When $z_i \neq 0$, we introduce a different method for simplification of the integration. We define the integral $W2(x_i, y_i, z_i) = I(x_i, y_i, z_i)$ and make a change of variables. Let $\alpha = r\cos\theta$, $\hat{\alpha} = r\sin\theta$, where $0 \le \theta \le \pi/2$, $0 \le r \le \infty$; the corresponding Jacobian transformation is $J = r$. The simplified form of $W2(x_i, y_i, z_i)$ is obtained by integrating over r

$$W2(x_i, y_i, z_i) = \int_0^{2\pi}\int_0^{\pi/2} \frac{\sin 2\theta}{4\pi|\wedge|^{1/2}} G(p_i, q_i)\, d\theta\, d\phi \tag{18a}$$

where, by definition

$$G(p,q) = \frac{1}{2p^2}\left(\frac{1}{2} - \frac{3q}{4\sqrt{2p+q^2}} - \frac{q^3}{4(2p+q^2)^{3/2}}\right) \tag{18b}$$

$$p_i = \frac{(\hat{\sigma}_x^2\cos^2\theta + \sigma_x^2\sin^2\theta) - R_c\sin 2\theta\cos\phi}{2|\wedge|^{1/2}} \tag{18c}$$

$$q_i = \frac{2\bar{\gamma}_b}{5\sigma_x^2}\left[\cos\theta(x_i\cos\varphi + y_i\sin\varphi) + z_i\sin\theta\right]. \tag{18d}$$

$$I(x, y, z, \bar{\gamma}_b, r, R_c) = \int_0^{\infty}\int_0^{\infty}\int_0^{2\pi} Q\left[\sqrt{\frac{2\bar{\gamma}_b}{5\sigma_x^2}}(x\alpha\cos\varphi + y\alpha\sin\varphi + z\hat{\alpha})\right] p(\alpha,\hat{\alpha},\varphi)\, d\varphi\, d\alpha\, d\hat{\alpha} \tag{15}$$

$$W1(x_i, y_i) = 0.5 - \int_{-\pi/2-\arctan^{-1} y_i/xi}^{\pi/2-\arctan^{-1} y_i/xi} \frac{\nu\cos\varphi}{8\pi|\wedge|^{1/2}\mu_2}\sqrt{\frac{\pi}{\mu_2}}\left\{\frac{\sqrt{\pi}}{4b^3} - \frac{1}{4\sqrt{\pi}}\left[\frac{1}{b^3}\tan^{-1}\frac{b}{a} - \frac{a}{b^2(a^2+b^2)}\right]\right\} d\varphi \tag{17a}$$

Combining (16) with (17) and (18), the BER for single-branch 16-QAM with decorrelation error can be expressed as

$$Pe = \frac{1}{8}\sum_{i=1}^{12} w_i I(x_i, y_i, z_i) = \frac{1}{8}\left[\sum_{i=1}^{4} w_i W1(x_i, y_i) + \sum_{i=1}^{8} w_i W2(x_i, y_i, z_i)\right]. \quad (19)$$

A more detailed derivation is available in [19]. The BER expression is then a combination of definite double and single integrals with finite limits. It is simpler than the results in [12], which are in the form of triple integrals and which take much longer to evaluate, particularly for large SNR values.

For future comparisons, we derive the BER of 16-QAM in Rayleigh fading with perfect channel estimation. The average BER can be obtained by averaging the conditional BER (conditioned on the SNR per bit) with respect to the SNR per bit, according to

$$P_e = \int_0^\infty P_e(\gamma_b) f(\gamma_b) d\gamma_b \quad (20)$$

where P_e is the average BER in slow fading, $P_e(\gamma_b)$ is the BER conditioned on the SNR per bit, γ_b, and $f(\gamma_b)$ is the pdf of the fading signal's SNR per bit. The pdf $f(\gamma_b)$ is given in [17, eq. (14.3–5)]. Rewriting (13) and (14) under the condition of perfect estimation, $\hat{\alpha} = \alpha$ and $\varphi = 0$ gives

$$P_M(e|\gamma_b) = Q\left(\sqrt{\frac{2\gamma_b}{5}}\right) + Q\left(3\sqrt{\frac{2\gamma_b}{5}}\right) \quad (21a)$$

$$P_L(e|\gamma_b) = \left[Q\left(\sqrt{\frac{2\gamma_b}{5}}\right) - Q\left(5\sqrt{\frac{2\gamma_b}{5}}\right)\right] + \left[Q\left(\sqrt{\frac{2\gamma_b}{5}}\right) + Q\left(3\sqrt{\frac{2\gamma_b}{5}}\right)\right]. \quad (21b)$$

Thus, the BER of 16-QAM in Rayleigh fading with perfect channel estimation can be obtained by combining (12) with (20) and (21) as

$$P_M = \frac{1}{2}\left[\frac{1}{2}(1-\mu_1) + \frac{1}{2}(1-\mu_2)\right] \quad (22a)$$

$$P_L = \frac{1}{2}\left\{\left[\frac{1}{2}(1-\mu_1) - \frac{1}{2}(1-\mu_3)\right] + \left[\frac{1}{2}(1-\mu_1) + \frac{1}{2}(1-\mu_2)\right]\right\} \quad (22b)$$

where, by definition

$$\mu_1 = \sqrt{\frac{2\bar{\gamma}_b}{5+2\bar{\gamma}_b}} \quad (22c)$$

$$\mu_2 = \sqrt{\frac{18\bar{\gamma}_b}{5+18\bar{\gamma}_b}} \quad (22d)$$

$$\mu_3 = \sqrt{\frac{50\bar{\gamma}_b}{5+50\bar{\gamma}_b}}. \quad (22e)$$

The derivation of (22) is very close to that in [1], except that our final result is expressed in terms of the SNR per bit, whereas the result in [1] is expressed in terms of symbol SNR.

Previously, the BER of single-branch reception 16-QAM in flat fading with imperfect channel estimation was derived in [12], but the results are approximations. As [12] neither identifies nor justifies that the analysis is approximate, we will clarify the analytical approach used there and contrast it with the analytical approach used here. Generally, the average BER can be calculated by averaging the conditional BER for the AWGN channel over the fading represented by the variables α, $\hat{\alpha}$, and φ. Hence

$$P_e = \int_0^\infty \int_0^\infty \int_0^{2\pi} P(e|\alpha, \hat{\alpha}, \varphi) p(\alpha, \hat{\alpha}, \varphi) d\varphi d\alpha d\hat{\alpha}. \quad (23)$$

First, note that it is well known that the amplitude and the phase of the Rayleigh fading channel are independent random variables. Thus

$$p(\alpha, \theta) = p(\alpha) p(\theta) \quad (24)$$

and the first-order jpdf factors into the product of the amplitude pdf and the phase pdf. However, and importantly, the envelope and phase random processes are not independent random processes. Conceptually, even though the single sample of the random amplitude process, α, is independent of the single sample of the random phase process, θ (both taken at the same time, t), multiple samples of the amplitude will not be independent of multiple samples of the phase (taken at multiple times). For example, we expect that amplitude "hits" (rapid changes from one sample to the next sample) will be accompanied by phase "hits." Experimental data reported in [20] shows this dependency. Thus, in the PSAM system, the channel estimate is a weighted sum of the estimates from the pilot symbols' channel fadings (3), and the jpdf of the amplitude of the channel gain α, and the amplitude of the channel gain estimate $\hat{\alpha}$, are not independent of the jpdf of the phase sample of the channel gain θ, and the phase sample of the channel gain estimate $\hat{\theta}$. In [12], the analysis and results are based on assuming the phase error $\theta - \hat{\theta}$, the amplitude α, and the amplitude estimate $\hat{\alpha}$, are independent. This treatment is equivalent to using the following equation:

$$P_e = \int_0^\infty \int_0^\infty \int_0^{2\pi} \int_0^{2\pi} P(e|\alpha, \hat{\alpha}, \theta, \hat{\theta}) p(\alpha, \hat{\alpha}) p(\theta, \hat{\theta}) d\theta d\hat{\theta} d\alpha d\hat{\alpha} \quad (25)$$

which is only an approximation. The exact form is

$$P_e = \int_0^\infty \int_0^\infty \int_0^{2\pi} \int_0^{2\pi} P(e|\alpha, \hat{\alpha}, \theta, \hat{\theta}) p(\alpha, \hat{\alpha}, \theta, \hat{\theta}) d\theta d\hat{\theta} d\alpha d\hat{\alpha}. \quad (26)$$

In [12], the jpdf $p(\alpha, \hat{\alpha}, \theta, \hat{\theta})$ has effectively been replaced by the product $p(\alpha, \hat{\alpha}) p(\theta, \hat{\theta})$. This conclusion can be drawn by careful scrutiny of [12, eqs. (38) and (40)]. This replacement requires that the amplitude samples $(\alpha, \hat{\alpha})$ are independent of the phase samples $(\theta, \hat{\theta})$. It is clear from the analysis in [13, Ch. 8] that $(\alpha, \hat{\alpha})$ and $(\theta, \hat{\theta})$ are not independent.

There is a second reason for which the BER results in [12] are only approximate. Even in the absence of noise and other system errors (for example, carrier recovery error or symbol timing error), the channel estimate is corrupted by an error that is Gaussian distributed. This error has its origin in the fact that the fading at an information symbol's time is decorrelated from the fading at a pilot symbol's time. Note particularly, that the BER depends on the location of the information symbol, since

the decorrelation depends on the location (in addition, other error sources may also depend on the location of the information symbol). These errors cause an error-rate floor which will determine the BER when the SNR is large. The analysis in [12] averages the parameters r ($r = \sigma_{\hat{x}}^2/\sigma_x^2$) and ρ (the correlation coefficient between α^2 and $\hat{\alpha}^2$) over l, the location of a symbol in a data-symbol frame, and then uses these averaged parameters in the BER equation. This approach is an approximation. The precise BER is obtained by averaging the BER conditioned on these parameters over the probabilities of these parameters, a more complex computation. The average BER can be obtained by averaging the conditional BERs over the locations of the information symbols in the frame.

IV. Diversity M-QAM

In the case of diversity M-QAM, imperfect channel estimation degrades the performance of the demodulation *and* degrades the performance of the diversity combining (recall that the weighting of the diversity branches in MRC requires estimates of the complex channel gains [21]). It is desired to find the BER of 16-QAM with MRC in Rayleigh fading, accounting both for the effect of imperfect channel estimation on the demodulation process and on the diversity combining. We assume that all the diversity branches are independent of each other. The derivation of the MRC diversity conditional BER follows the same method given in [17, Ch.5], that was used for the single-branch case in Section III and illustrated in Figs. 2 and 3, but is modified to include the effect of the MRC diversity. Full details are available in [19]. We start from (13) and (14) and alter these equations to account for diversity, fading, and channel estimation error, as well as ISI. To do so, we define a useful ancillary parameter t_i and then condition the BER on t_i, giving

$$P(e|t_i) = \frac{1}{8}\sum_{i=1}^{12} w_i Q \cdot \left(\sqrt{A \frac{\left[\sum_{m=0}^{M-1} \alpha_m \hat{\alpha}_m (x_i \cos\varphi_m + y_i \sin\varphi_m) + z_i \hat{\alpha}_m^2\right]^2}{\sum_{m=0}^{M-1} \hat{\alpha}_m^2}} \right) \tag{27a}$$

$$A = \left(\frac{d}{\sigma_n}\right)^2 = \frac{2\bar{\gamma}_b}{5\sigma_x^2} \tag{27b}$$

$$t_i = \frac{\sum_{m=0}^{M-1} \hat{\alpha}_m \left[(\alpha_m x_i \cos\varphi_m + \alpha_m y_i \sin\varphi_m) + z_i \hat{\alpha}_m\right]}{\sqrt{\sum_{m=0}^{M-1} \hat{\alpha}_m^2}} \tag{27c}$$

where α_m, $\hat{\alpha}_m$, and φ_m are the fading channel amplitude, channel amplitude estimate, and the phase error on the mth diversity branch, respectively, M is the number of diversity branches, and the coefficients w_i, x_i, y_i, z_i are again listed in Table I. The parameter, t_i, is clarified as follows. In the single-branch case, $M = 1$ and the BER of the 16-QAM in the absence of fading is given by (13) and (14). In the case of diversity, $M > 1$ and t_i corresponds to the ith term in a sum of weighted terms, each term being a $Q(\cdot)$ function, as in (13) and (14). The decision statistic of the mth diversity branch includes the transmitted signal distorted by the phase error, $\alpha_m x_i \cos\varphi_m$, the ISI, $\alpha_m y_i \sin\varphi_m$, caused by phase error, and the decision boundary information represented by $z_i\hat{\alpha}_m$, which is determined by the amplitude estimate.

We need the pdf of t_i. The derivation of the pdf of t_i follows the analysis described in [22], but in contrast to the analysis in [22] where the variances of a fading quadrature component and its estimate are equal, here the variances of a fading quadrature component and its estimate are different. The case where they are equal models noiseless estimation and, thus, only the effects of decorrelation are accounted for in the analysis of [22]. We extend the analysis of [22] to include channel estimation error originating from both decorrelation and noise. Let the variance of a fading quadrature component and its estimate be σ_x and $\sigma_{\hat{x}}$, respectively. The amplitude of the estimate, $\hat{\alpha}_m$, is Rayleigh distributed, and its pdf is given by [17, eq. (2-1–128)]

$$p(\hat{\alpha}_m) = \frac{\hat{\alpha}_m}{\sigma_{\hat{x}}^2} \exp\left(-\frac{\hat{\alpha}_m^2}{2\sigma_{\hat{x}}^2}\right). \tag{28}$$

Then the conditional pdf of α_m, φ_m given $\hat{\alpha}_m$ is

$$p(\alpha_m, \varphi_m|\hat{\alpha}_m) = \frac{p(\alpha_m, \hat{\alpha}_m, \varphi_m)}{p(\hat{\alpha}_m)} \tag{29}$$

where $p(\alpha_m, \hat{\alpha}_m, \varphi_m)$ is given in (4a).

Define

$$\alpha_m \cos\varphi_m = u_m + \frac{R_c \hat{\alpha}_m}{\sigma_{\hat{x}}^2} \tag{30a}$$

$$\alpha_m \sin\varphi_m = v_m + \frac{R_{cs} \hat{\alpha}_m}{\sigma_{\hat{x}}^2} \tag{30b}$$

$$du_m dv_m = \alpha_m d\alpha_m d\varphi_m \tag{30c}$$

and (28)–(30) yield

$$p(u_m, v_m|\hat{\alpha}_m) = \frac{\sigma_{\hat{x}}^2}{2\pi\wedge^{1/2}} \exp\left[-\frac{\sigma_{\hat{x}}^2}{2\wedge^{1/2}}(u_m^2 + y_m^2)\right] \tag{31}$$

where R_c, R_{cs}, and $\wedge$ were defined in Section II. It can be shown from (31) that u_m and v_m are independent of each other, and independent of $\hat{\alpha}_m$ [22]. Each of them has a zero-mean Gaussian distribution with variance $\wedge^{1/2}/\sigma_{\hat{x}}^2$. Now define

$$u = \frac{\sum_{m=0}^{M-1} \hat{\alpha}_m u_m}{\sqrt{\sum_{m=0}^{M-1} \hat{\alpha}_m^2}} \tag{32a}$$

$$v = \frac{\sum_{m=0}^{M-1} \hat{\alpha}_m v_m}{\sqrt{\sum_{m=0}^{M-1} \hat{\alpha}_m^2}} \tag{32b}$$

$$U = \frac{R_c}{\sigma_{\hat{x}}^2}\left(\sum_{m=0}^{M-1} \hat{\alpha}_m^2\right)^{1/2}. \tag{32c}$$

It is shown in [22] that u and v are also Gaussian distributed with variance $\wedge^{1/2}/\sigma_{\hat{x}}^2$ and are independent of $\hat{\alpha}_m$. The parameter U has a chi density [14, eq. (5–25)] with $2M$ degrees of freedom,

and each degree of freedom has a variance σ^2. Note that u and U are independent of each other [22]. We rewrite t_i from (27c) as

$$\begin{aligned} t_i &= x_i(u+U) + y_i v + z_i \left(\sum_{m=0}^{M-1} \hat{\alpha}_m^2\right)^{1/2} \\ &= x_i(u+U_i') + y_i v \\ &= x_i\mu_i + y_i v \end{aligned} \tag{33a}$$

where

$$U_i' = \left(\frac{R_c}{\sigma_{\hat{x}}^2} + \frac{z_i}{x_i}\right)\left(\sum_{m=0}^{M-1} \hat{\alpha}_m^2\right)^{1/2}. \tag{33b}$$

Summarizing, the pdfs of u, U, and v are given by

$$p(u) = \frac{\sigma_{\hat{x}}}{\sqrt{2\pi\wedge^{1/2}}} \exp\left[-\frac{\sigma_{\hat{x}}^2}{2\wedge^{1/2}}u^2\right] \tag{34a}$$

$$p(v) = \frac{\sigma_{\hat{x}}}{\sqrt{2\pi\wedge^{1/2}}} \exp\left[-\frac{\sigma_{\hat{x}}^2}{2\wedge^{1/2}}v^2\right] \tag{34b}$$

$$p(U) = \frac{2U^{2M-1}\exp\left(-\frac{U^2}{2\sigma^2}\right)}{2^M\sigma^{2M}\Gamma(M)} \tag{34c}$$

where $\sigma^2 = R_c^2/\sigma_{\hat{x}}^2$, and the pdf of U_i' is given by

$$p(U_i') = \frac{2U_i'^{2M-1}\exp(-\frac{U_i'^2}{2\sigma_i^2})}{2^M\sigma_i^{2M}\Gamma(M)} \tag{34d}$$

where $\sigma_i^2 = \left(R_c/\sigma_{\hat{x}}^2 + z_i/x_i\right)^2\sigma_{\hat{x}}^2$, and then the pdf of $u+U_i'$ is found as

$$\begin{aligned} &p_{u+U_i'}(\mu_i) \\ &\quad= \int_0^\infty p_u(\mu_i - U_i')p_{U_i'}(U_i')dU_i' \\ &\quad= \frac{\sqrt{2}\sigma_{\hat{x}}\exp(-\frac{\sigma_{\hat{x}}^2\mu_i^2}{2\wedge^{1/2}})}{2^M\sqrt{\pi\wedge^{1/2}}\sigma_i^{2M}\Gamma(M)} \\ &\qquad\cdot\int_0^\infty U_i'^{2M-1}\exp(-\beta_i U_i'^2 - \lambda_i U_i')dU_i' \end{aligned} \tag{34e}$$

where

$$\beta_i = \frac{1}{2\sigma_i^2} + \frac{\sigma_{\hat{x}}^2}{2\wedge^{1/2}} \tag{34f}$$

$$\lambda_i = -\frac{\sigma_{\hat{x}}^2\mu_i}{\wedge^{1/2}}. \tag{34g}$$

Equation (34e) can be simplified using [23, eq. (3.462)]. Thus

$$\begin{aligned} p(\mu_i) &= \frac{\sqrt{2}\sigma_{\hat{x}}\Gamma(2M)}{2^{2M}\sqrt{\pi\wedge^{1/2}}\sigma_i^{2M}\beta_i^M\Gamma(M)} \\ &\cdot\exp\left[-\left(\frac{1}{2} - \frac{\sigma_{\hat{x}}^2}{8\wedge^{1/2}\beta_i}\right)\frac{\sigma_{\hat{x}}^2\mu_i^2}{\wedge^{1/2}}\right] D_{-2M}\left(\frac{-\sigma_{\hat{x}}^2\mu_i}{\sqrt{2\wedge\beta_i}}\right) \end{aligned} \tag{35}$$

where $D_\nu(x)$ is the parabolic cylinder function defined at [22, eq. (42)].

Since x_i, y_i, and z_i are real numbers and μ_i and v are independent, the BER of 16-QAM with MRC can be written as

$$Pe = \frac{1}{8}\sum_{i=1}^{12}\int_{-\infty}^{\infty}\int_{-\infty}^{\infty} w_i Q\left[\sqrt{A}(x_i\mu_i + y_i v)\right]p(\mu_i)p(v)d\mu_i dv. \tag{36}$$

Equation (36) is a double integral in two variables, each of which has doubly infinite range. Making the variable changes, $\mu_i = r_i\cos\theta_i$ and $v = r_i\sin\theta_i$, where $0 \le \theta_i \le 2\pi$, $0 \le r_i \le \infty$, the corresponding Jacobian of the transformation is $J = r_i$. Then (36) can be written as shown in (37) at the bottom of the page, with the coefficients w_i, x_i, y_i, and z_i given in Table I. Using (37), P_e can be calculated numerically for a given order of diversity M and given frame length L, as well as given symbol location, l.

The BER of 16-QAM in Rayleigh fading with perfect channel estimation is derived here for later comparisons. It is well known that for the case of perfect channel estimation, the MRC output signals on both the I and Q branches are real, thus, the conditional BER depends only on the SNR [17], [21]. The BER of 16-QAM with MRC and perfect channel estimation is obtained according to (20) by combining $f(\gamma_b)$ given in [17, eq. (14.3–7)] with $P_M(e|\gamma_b)$ and $P_L(e|\gamma_b)$ given in (21), where

$$\begin{aligned} P_M = \frac{1}{2}\Bigg\{&\left[\frac{1}{2}(1-\mu_1)\right]^M\sum_{m=0}^{M-1}\binom{M-1+m}{m}\left[\frac{1}{2}(1+\mu_1)\right]^m \\ &+\left[\frac{1}{2}(1-\mu_2)\right]^M\sum_{m=0}^{M-1}\binom{M-1+m}{m}\left[\frac{1}{2}(1+\mu_2)\right]^m\Bigg\} \end{aligned} \tag{38a}$$

$$\begin{aligned} P_L = \frac{1}{2}\Bigg\{&\left[\frac{1}{2}(1-\mu_1)\right]^M\sum_{m=0}^{M-1}\binom{M-1+m}{m}\left[\frac{1}{2}(1+\mu_1)\right]^m \\ &-\left[\frac{1}{2}(1-\mu_3)\right]^M\sum_{m=0}^{M-1}\binom{M-1+m}{m}\left[\frac{1}{2}(1+\mu_3)\right]^m \\ &+\left[\frac{1}{2}(1-\mu_1)\right]^M\sum_{m=0}^{M-1}\binom{M-1+m}{m}\left[\frac{1}{2}(1+\mu_1)\right]^m \\ &+\left[\frac{1}{2}(1-\mu_2)\right]^M\sum_{m=0}^{M-1}\binom{M-1+m}{m}\left[\frac{1}{2}(1+\mu_2)\right]^m\Bigg\}. \end{aligned} \tag{38b}$$

Note that (38) assumes perfect channel estimation both for the demodulation and for the channel weighting in the maximal ratio diversity combining. To the best of the authors' knowledge, this expression is new and different from other results in the literature. [24] gives a result for the BER of MRC QAM in Rayleigh fading with perfect channel estimation, but this result is an approximation. It is obtained by dividing the SER by the

$$Pe = \frac{1}{8}\sum_{i=1}^{12}\int_0^\infty\int_0^{2\pi} w_i r_i Q\left[\sqrt{A}(x_i r_i\cos\theta_i + y_i r_i\sin\theta_i)\right]p(r_i\cos\theta_i)p(r_i\sin\theta_i)d\theta_i dr_i \tag{37}$$

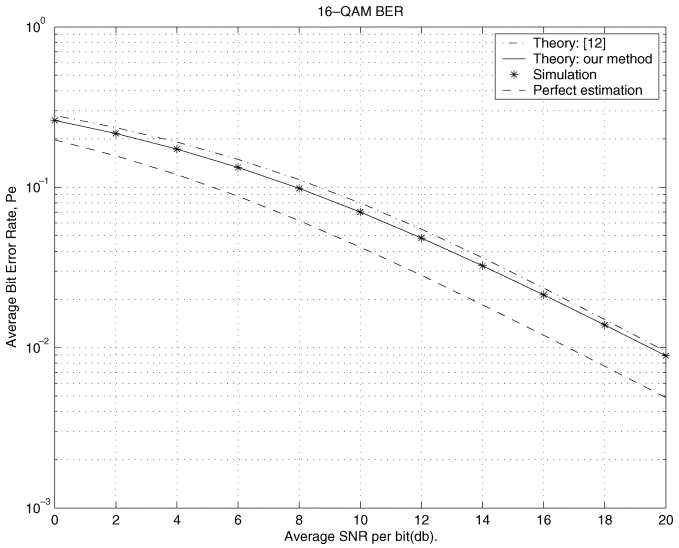

Fig. 4. BER performance of single-branch 16-QAM with a Hamming windowing applied to the sinc interpolator for $L = 15$, $K = 30$, and $f_D T_s = 0.03$ and averaged over symbol location l.

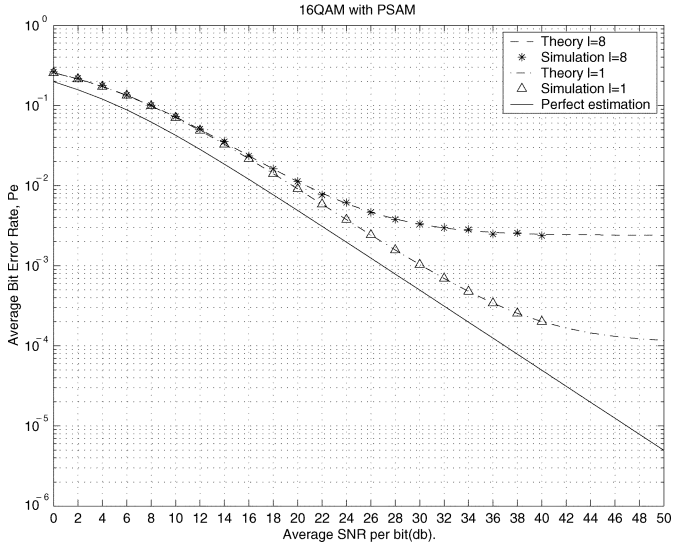

Fig. 5. 16-QAM BER performance of a single-branch receiver with a rectangular window applied to the sinc interpolator for $L = 15$, $K = 30$, and $f_D T_s = 0.03$; the parameter l is the symbol location in one frame.

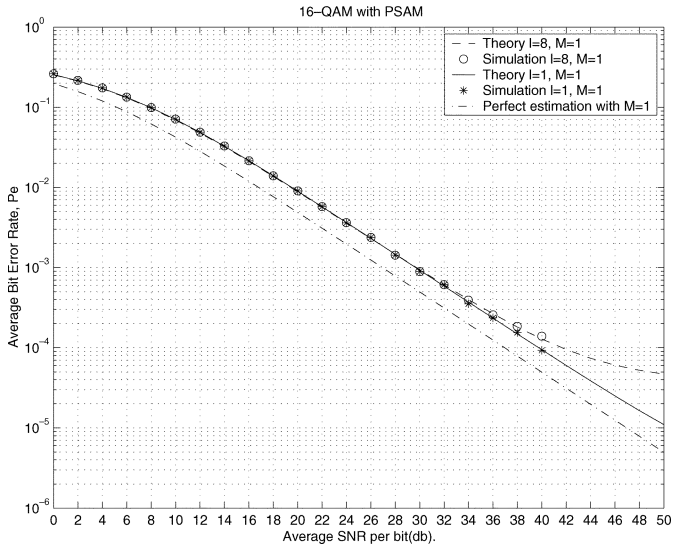

Fig. 6. 16-QAM BER performance of a single-branch receiver with a Hamming window applied to the sinc interpolator for $L = 15$, $K = 30$, and $f_D T_s = 0.03$; the parameter l is the symbol location in one frame.

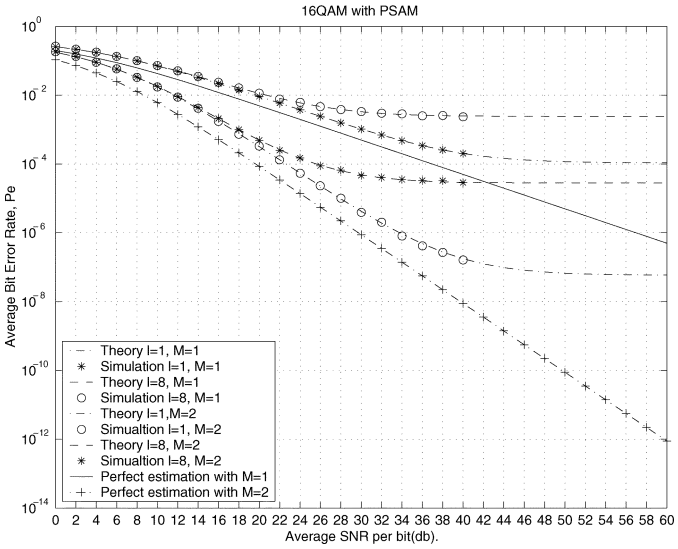

Fig. 7. BER performance of 16-QAM with dual-branch diversity and rectangular windowing applied to the sinc interpolator for $L = 15$, $K = 30$, and $f_D T_s = 0.03$; M is the number of diversity branches and l is the symbol location in one frame.

number of bits per symbol. Obtaining the exact result requires accounting for the specific (different) number of bit errors occurring for each particular symbol error, as done here.

Our examples in the next section will consider the BERs at symbol location $l = 1$ and $l = 8$, the sensitivity of the BER results to the choice of windows used in the pilot-symbol interpolation filter, and the sensitivity of diversity systems to channel estimation errors. Comparisons between our results and the results obtained in [12] are included. We also test the validity of our results for large values of $f_D T$.

V. Examples

All the numerical results in this section were obtained using Mathematica, and the simulations were implemented in Matlab. The simulator in [25] is used to generate complex samples from a Rayleigh flat-fading channel with Doppler shift. The high statistical quality of this simulator is certified in [25] and [26]. In Figs. 4–8, we set the system parameters for both numerical calculation and simulation as frame length $L = 15$, interpolation order $K = 30$ with $k_1 = 14$ and $k_2 = 15$, normalized Doppler spread $f_D T = 0.03$, and fading variance $\sigma_x^2 = 1$. A sinc interpolator [10] is used as estimator filter. The BERs resulting when a rectangular window and a Hamming window are applied to the sinc interpolator function are both calculated for comparison.

Fig. 4 compares the average BERs averaging over the symbol location l obtained by our method and the method in [12] in the SNR range 0–20 dB. It shows a distinct difference between

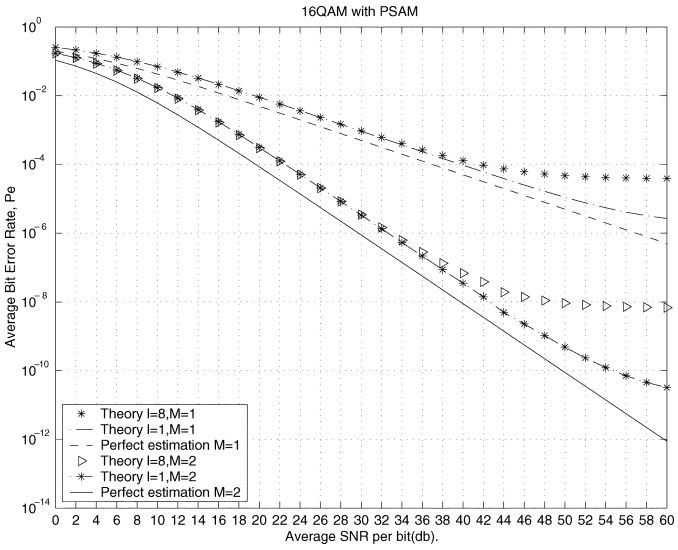

Fig. 8. BER performance of 16-QAM with dual-branch diversity and Hamming windowing applied to the sinc interpolator for $L = 15$, $K = 30$, and $f_D T_s = 0.03$; M is the number of diversity branches and l is the symbol location in one frame.

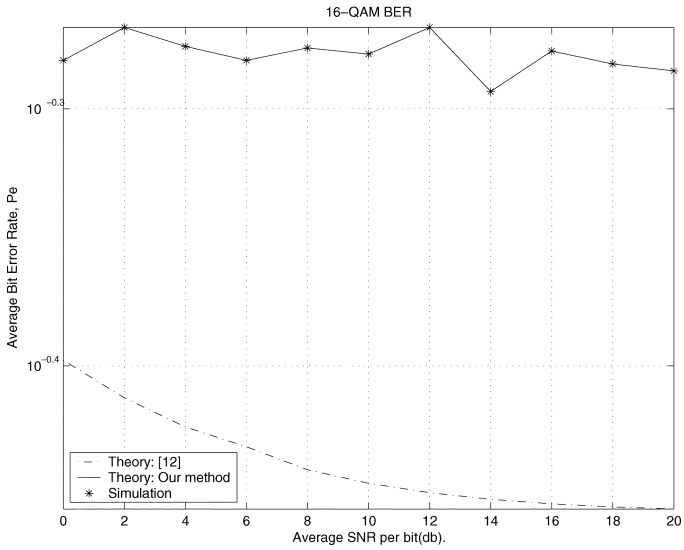

Fig. 9. BER performance of single-branch 16-QAM with Hamming windowing applied to the sinc interpolator for $L = 15$, $K = 30$, and $f_D T_s = 0.1$ with symbol location at $l = 8$.

the two curves at small SNR values which diminishes with increasing SNR. For example, at $P_b = 10^{-1}$, the difference is 0.74 dB; at $P_b = 10^{-2}$, the difference is 0.29 dB.

Figs. 5 and 6 show the BERs of 16-QAM for single-branch reception with a rectangular window and a Hamming window applied to the sinc interpolator, respectively, as a function of the average SNR per bit. Both theoretical and simulation results for the $l = 1$ case and the $l = 8$ case, as well as the BER for perfect channel estimation, are presented. Note first that our theoretical results and simulation results are in excellent agreement. The performance using a rectangular window is significantly worse than that using a Hamming window. One sees from comparison of Fig. 6 with Fig. 5 that the abrupt truncation of the rectangular window severely degrades performance by causing decorrelation relative to the Hamming window. The BER at symbol location $l = 8$ exhibits error-rate floors that are in evidence for values of SNR greater than 30 and 46 dB for the rectangular window and the Hamming window, respectively. The error floors are caused by decorrelation which originates in the channel variations and in the channel estimation filtering. The results also show that the error-rate floor caused by decorrelation is greater for information symbols more distant from the pilot symbols, as expected.

Figs. 7 and 8 show the BER performance of dual-branch MRC ($M = 2$) diversity. The BER performance without diversity is also shown for comparison. Simulation results shown for the case with a rectangular window are consistent with the theoretical results. Simulation results are not given for dual-branch MRC with a Hamming window, owing to the time needed to generate them. The BER performance with MRC is much better than without diversity, as expected. Note particularly that the BER floor occurring for $l = 8$ is lowered by almost two orders of magnitude by the use of dual diversity. However, the performance of 16-QAM with diversity degrades more than that of a single-branch system, due to the decorrelation. For example, in Fig. 7, at SNR $= 30$ dB with $l = 8$, the BER is increased by a factor of 6.6 (from 4.96×10^{-4} to 3.3×10^{-3}) for the system without diversity, while the BER is increased by a factor of 54.6 (from 8.82×10^{-7} to 4.81×10^{-5}) for the dual diversity system; in Fig. 8, at SNR $= 50$ dB with $l = 8$, the BER is increased by a factor of 9.45 (from 4.97×10^{-6} to 4.7×10^{-5}) for the system without diversity, while the BER is increased by a factor of 103 (from 8.85×10^{-11} to 9.19×10^{-9}) for the dual diversity system. This is expected, since the channel estimation error degrades the diversity combining as well as degrading the coherent demodulation.

The validity of the results will be tested by using large values of $f_D T$. Further, the validity of the results will be tested by cases where the probability of the phase error ϕ being greater than 0.5π is significant. Note that the probability of ϕ being greater than 0.5π depends on the quality of the channel estimate. In particular, the frame length L of the interpolation filter should be chosen such that the pilot symbols can adequately track the Doppler frequency shift. When this is the case, the probability of ϕ being greater than 0.5π is kept small. The validity of our analysis is, thus, best tested by choosing the PSAM parameters such that the value of $f_D T$ is outside the range of the tracking of the interpolation filter. We do this test in Figs. 9 and 10. In both of the figures, we present our numerical results, results from [12], and simulation results.

In Fig. 9, $f_D T$ is set as 0.1 and the frame length remains 15. In this case, the channel changes faster than the pilot-symbol insertion rate, and the interpolator can not provide good channel information. The detector works poorly. The simulation results are in agreement with our numerical results. Fig. 9 also shows that the methods in [12] can not provide good approximation in this situation. In Fig. 10, $f_D T$ is set as 0.1 and the frame length is changed to 4. As expected, the detector now works well, since it receives good channel estimates. Again, our theoretical results agree with the simulation results. Figs. 9 and 10 confirm the correctness of our analytical results.

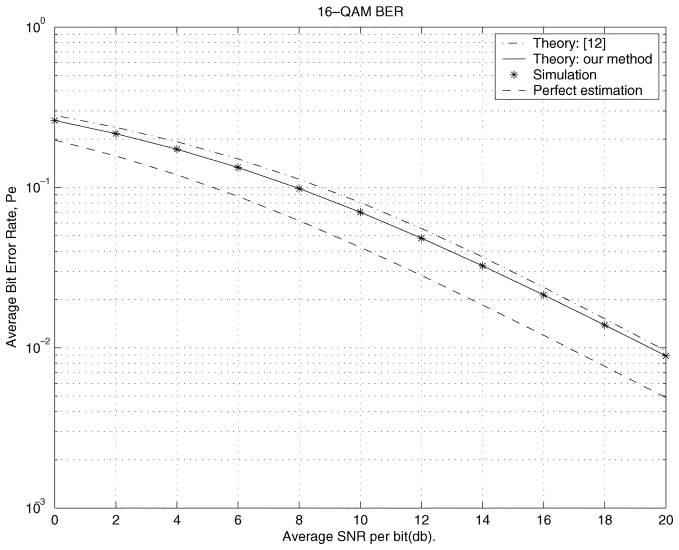

Fig. 10. BER performance of single-branch 16-QAM with Hamming windowing applied to the sinc interpolator for $L = 4$, $K = 30$, and $f_D T_s = 0.1$ with symbol location at $l = 8$.

VI. Conclusion

The exact BER of 16-QAM when used with PSAM channel estimation has been derived for AWGN channels and Rayleigh fading channels with and without diversity. The effects of imperfect channel estimation on the BER have been studied. Both noise and estimator decorrelation effects have been examined. It was shown that the channel estimation error can have a serious effect on the received data BER and that the decorrelation causes an error-rate floor. The method can be applied to general M-QAM with minor modification but more cumbersome definitions, notations, and development. It can also be applied to other estimation techniques if the channel estimate is jointly Gaussian with the channel gain.

References

[1] L. Hanzo, T. Webb, and T. Keller, *Single- and Multi-Carrier Quadrature Amplitude Modulation: Principles and Applications for Personal Communications, WLAN's and Broadcasting*. Chichester, U.K.: Wiley, 2002.

[2] P. K. Vitthaladevuni and M.-S. Alouini, "A recursive algorithm for the exact BER computation of generalized hierarchical QAM constellations," *IEEE Trans. Inform. Theory*, vol. 49, pp. 297–307, Jan. 2003.

[3] C.-J. Kim, Y.-S. Kim, G.-Y. Jeong, J.-K. Mun, and H.-J. Lee, "SER analysis of QAM with space diversity in Rayleigh fading channels," *ETRI J.*, vol. 17, no. 4, pp. 15–25, Jan. 1996.

[4] A. Annamalai, C. Tellambura, and V. K. Bhargava, "Exact evaluation of maximal-ratio and equal-gain diversity receivers for M-ary QAM on Nakagami fading channels," *IEEE Trans. Commun.*, vol. 47, pp. 1335–1344, Sept. 1999.

[5] X. Dong, N. C. Beaulieu, and P. H. Wittke, "Signaling constellations for fading channels," *IEEE Trans. Commun.*, vol. 47, pp. 703–714, May 1999.

[6] M. K. Simon and M.-S. Alouini, "A unified approach to the performance analysis of digital communication over generalized fading channels," *Proc. IEEE*, vol. 86, pp. 1860–1877, Sept. 1998.

[7] M. G. Shayesteh and A. Aghamohammadi, "On the error probability of linearly modulated signals on frequency-flat Ricean, Rayleigh, and AWGN channels," *IEEE Trans. Commun.*, vol. 43, pp. 1454–1466, Feb. 1995.

[8] A. J. Goldsmith and S.-G. Chua, "Variable-rate variable-power MQAM for fading channels," *IEEE Trans. Commun.*, vol. 45, pp. 1218–1230, Oct. 1997.

[9] J. K. Cavers, "An analysis of pilot-symbol-assisted modulation for Rayleigh fading channels," *IEEE Trans. Veh. Technol.*, vol. 40, pp. 1389–1399, Nov. 1991.

[10] Y.-S. Kim, C.-J. Kim, G.-Y. Jeong, Y.-J. Bang, H.-K. Park, and S. S. Choi, "New Rayleigh fading channel estimator based on PSAM channel sounding technique," in *Proc. IEEE Int. Conf. Communications*, June 1997, pp. 1518–1520.

[11] K. Yu, J. Evans, and I. Collings, "Performance analysis of pilot-symbol-aided QAM for Rayleigh fading channels," in *Proc. IEEE Int. Conf. Communications*, vol. 3, Apr. 2002, pp. 1731–1735.

[12] X. Tang, M.-S. Alouini, and A. J. Goldsmith, "Effect of channel estimation error on M-QAM BER performance in Rayleigh fading," *IEEE Trans. Commun.*, vol. 47, pp. 1856–1864, Dec. 1999.

[13] W. Davenport and W. Root, *Introduction to the Theory of Random Signals and Noise* . New York: IEEE Press, 1987.

[14] A. Papoulis and S. U. Pillai, *Probability, Random Variables and Stochastic Processes*, 4th ed. Boston, MA: McGraw-Hill, 2002.

[15] G. L. Stuber, *Principles of Mobile Communication*, 2nd ed. Norwell, MA: Kluwer, 2001.

[16] *Handbook of Mathematical Functions with Formulas, Graphs, and Mathematical Tables*, M. Abramowitz and I. A. Stegun, Eds., Dover, New York, 1974.

[17] J. G. Proakis, *Digital Communications*, 4th ed. New York: McGraw-Hill, 2001.

[18] B. Sklar, *Digital Communications: Fundamentals and Applications*, 2nd ed. Upper Saddle River, NJ: Prentice-Hall, 2001.

[19] L. Cao, "Exact error rate analysis of MRC diversity with channel estimation error," M.Sc. thesis, Univ. Alberta, Edmonton, AB, Canada, 2003.

[20] M. Fattouche and H. Zaghloul, "Equalization of $\pi/4$ offset DQPSK transmitted over flat fading channels," in *IEEE Int. Conf. Communications*, vol. 1, June 14–18, 1992, pp. 296–298.

[21] D. G. Brennan, "Linear diversity combining techniques," *Proc. IRE*, vol. 47, pp. 1075–1102, June 1959.

[22] M. J. Gans, "The effect of Gaussian error in maximal ratio combiners," *IEEE Trans. Commun. Technol.*, vol. COM-19, pp. 492–500, Aug. 1971.

[23] I. S. Gradshteyn and I. M. Ryzhik, *Table of Integrals, Series, and Products*, 6th ed. San Diego, CA: Academic, 2000.

[24] C.-J. Kim, Y.-S. Kim, G.-Y. Jeong, and H.-J. Lee, "BER analysis of QAM with MRC space diversity in Rayleigh fading channel," in *Proc. PIMRC*, Sept. 1995, pp. 482–485.

[25] D. J. Young and N. C. Beaulieu, "The generation of correlated Rayleigh random variates by inverse discrete Fourier transform," *IEEE Trans. Commun.*, vol. 48, pp. 1114–1127, July 2000.

[26] ——, "Power margin quality measures for correlated random variates derived from the normal distribution," *IEEE Trans. Inform. Theory*, vol. 49, pp. 241–252, Jan. 2003.

Lingzhi Cao received the B.S. degree in electronics engineering from Shanghai Jiaotong University, Shanghai, China, in 1999, and the M.S. degree in electrical engineering from University of Alberta, Edmonton, AB, Canada, in 2003.

She was with Shanghai Bell Alcatel Mobile Communication System Company, Shanghai, China, as a Network Optimization Engineer from July 1999 to August 2001. She was involved in several major optimization projects and techniques functionalities testing, such as frequency-hopping system testing, DCS1800 and GSM900 multiband network testing, and concentric cells testing. She is familiar with the GSM network, especially the GSM signaling procedure, handover algorithm, cell selection/reselection algorithm and related parameters. She is currently with the iCORE Wireless Communication Laboratory, University of Alberta. Her research interests are in the areas of fading channel, diversity, channel estimation, and modulation.

Norman C. Beaulieu (S'82–M'86–SM'89–F'99) received the B.A.Sc. (honors), M.A.Sc., and Ph.D. degrees in electrical engineering from the University of British Columbia, Vancouver, BC, Canada, in 1980, 1983, and 1986, respectively.

He was a Queen's National Scholar Assistant Professor with the Department of Electrical Engineering, Queen's University, Kingston, ON, Canada, from September 1986 to June 1988, an Associate Professor from July 1988 to June 1993, and a Professor from July 1993 to August 2000. In September 2000, he became the iCORE Research Chair in Broadband Wireless Communications at the University of Alberta, Edmonton, AB, Canada, and in January 2001, the Canada Research Chair in Broadband Wireless Communications. His current research interests include broadband digital communications systems, fading channel modeling and simulation, interference prediction and cancellation, decision-feedback equalization, and space–time coding.

Dr. Beaulieu is a Member of the IEEE Communication Theory Committee and served as its Representative to the Technical Program Committee of the 1991 International Conference on Communications and as Co-Representative to the Technical Program Committee of the 1993 International Conference on Communications and the 1996 International Conference on Communications. He was General Chair of the Sixth Communication Theory Mini-Conference in association with GLOBECOM 97 and Co-Chair of the Canadian Workshop on Information Theory 1999. He has been an Editor for Wireless Communication Theory of the IEEE TRANSACTIONS ON COMMUNICATIONS since January 1992, and was Editor-in-Chief from January 2000 to December 2003. He served as an Associate Editor for Wireless Communication Theory of the *IEEE Communications Letters* from November 1996 to August 2003. He has also served on the Editorial Board of the *Proceedings of the IEEE* since November 2000. He received the Natural Science and Engineering Research Council of Canada (NSERC) E. W. R. Steacie Memorial Fellowship in 1999. He was awarded the University of British Columbia Special University Prize in Applied Science in 1980 as the highest standing graduate in the faculty of Applied Science. He is a Fellow of The Royal Society of Canada.